ROTOR LOSSES IN AXIAL-FLUX PERMANENT-MAGNET MACHINES WITH NON-OVERLAPPED WINDINGS

J.L. Colton, D.J. Patterson, J. Hudgins

Electrical Engineering Department, University of Nebraska, Lincoln, NE 68588-0511, USA
E-mail of corresponding author: colton.jessica@huskers.unl.edu
Telephone: +1 402 472 5826

Keywords: axial flux, rotor loss, non-overlapped windings, permanent-magnet machines, finite element analysis.

Abstract

A characterization of the rotor losses in single-sided axial-flux permanent-magnet (AFPM) machines fitted with non-overlapped windings (NOW) is presented in this paper, through experimental validation of finite element analysis (FEA) estimates. A literature review detailing the previous work done in the area of rotor loss estimation is given and the approaches taken by the authors to model the AFPM geometry, especially for 2D FEA, are detailed. Finally, the difficult issue of validating the FEA results with experimental data is addressed specifically with a prototype 24-slot/20-pole single-sided AFPM fitted with a single-layer (SL) set of NOW.

1 Introduction

In recent years, the use of NOW schemes, in which a coil spans a single tooth, has largely replaced that of traditional full-pitched windings in high performance electric machine designs. Inherent in these winding designs are many benefits including reduced copper mass (and loss), better machine manufacturability, decreased cogging torque and performance enhancements in terms of fault-tolerance and flux-weakening capabilities, just to name a few. However, the use of NOW also comes with penalties resulting from a harmonic-rich airgap MMF waveform that manifests itself as reductions in winding factors and increased rotor losses when compared with machines equipped with traditional windings. It is this latter penalty that is of interest in this paper.

The investigation of eddy current rotor losses in single-sided AFPM machines is of particular interest because these machines are typically designed with open slots and solid steel back-plates in addition to being fitted with NOW. One goal of this paper is then to determine the fractions of total rotor loss that result from stator slotting ($P_{r,slot}$) and MMF space harmonics ($P_{r,NOW}$) respectively.

The focus on experimental measurement of these losses may initially seem frivolous in this age of rich computing resources and intelligent FEA software; however, it is the authors' opinion this experimental evidence is important specifically when AFPM machines are considered with the following reasoning. 2D FEA is a common tool in the field of machine design and has been shown to yield reasonable estimations of actual machine performance when applied correctly. However, unlike the radial-flux (RF) geometry, AF machines are difficult to model in two-dimensions and if this is done, there are inherent errors in the model due to geometrical approximations. It is possible to use 3D analysis, however this approach is substantially more time and resource consuming than its 2D counterpart, so it is often not a good option until a design has been more established. Additionally, it has been the authors' experience that 3D FEA computations are very sensitive to meshing operations and time stepping (when the transient solver is employed).

A useful approach to modeling the AFPM machine in 2D will be described subsequently and the experimental measurements are then used to typify the magnitudes of errors that can be expected from the model approximations. The process of experimentally isolating the rotor loss measurements is not trivial and so will occupy the majority of this paper.

2 Literature Review

As described in the introduction, the computation of rotor losses in PM machines has gained interest recently due to the almost exclusive implementation of NOW schemes in modern machine designs. The purpose of this section is to identify the state of research in describing and defining the losses.

In [2], Bianchi et al. calculated the rotor losses due to MMF harmonics of RFPM machines with NOW by using analytical techniques to simplify a 2D FEA procedure. The stator-induced harmonics were transformed into a rotor reference frame frequency and applied to current sheets in the model. The rotor losses for an extensive list of slot-pole combinations for a particular machine size were tabulated and the main result from this work is that the single-layer (SL) winding schemes exhibit increased loss due to richer harmonic content than their double-layer (DL) counterparts. It should be noted that the effects of stator slotting and any time harmonics in the stator current waveform were neglected.

A method of calculating rotor eddy-current losses, employing both 2D and 3D FEA was introduced in [7], by Saban and Lipo, for a high-speed RF machine. The main idea of the

technique is that 2D FEA can be used to determine a rotor-referenced current sheet, which mimics the effects of the stator MMF waveform, to serve as an input to a 3D model. The method presented takes into account time harmonics, space harmonics and the effects of slotting in the MMF distribution; however, no loss calculation results were presented.

An analytical technique for calculating rotor back-iron eddy-current losses due to MMF space harmonics in a RF machine was presented in [6] by Polinder et al. in contrast to the FEA methods that had thus far been developed. The technique is based on decomposition of the MMF distribution (with slotting incorporated by application of the Carter coefficient) into its harmonic components and calculating the corresponding harmonic flux density magnitudes to be used in the loss calculations. Jassal et al. used this approach in [4] to compare rotor back-iron loss between three different NOW machines and a machine with traditional windings, confirming that the rotor loss for the NOW machines all exceed that of the traditional machine.

Han et al. examined rotor eddy-current losses in [3] for an interior permanent-magnet (IPM) machine using a similar approach as was suggested in [6]; except that here the loss calculation was performed via 2D FEA. The study identified that the parameters with the greatest impact on these losses are the magnitude of the fundamental component of the stator MMF, the stator slot pitch and the yoke pitch between the rotor barrier ends.

In [5], Nuscheler presented a 2D analytical model for calculating rotor eddy-current losses in a RFPM machine that is derived directly from Maxwell's equations. Multiple instances of two different slot-pole combination machines, each with varying degrees of rotor lamination and magnet segmentation, were analyzed with the model solely in terms of the harmonic with the highest magnitude (excluding the main harmonic). It was determined that lamination of the rotor yoke increases the eddy-current losses in the magnets, but that loss can be mitigated by segmentation of the magnets.

A study involving experimental validation of analytical rotor eddy-current calculations for an AF machine was performed in [1] by Alberti et al. The analytical method is based on solutions of Maxwell's equations in two dimensions and the losses are calculated by considering the contribution of each harmonic separately. The authors were careful to include the effects of stator slotting, as AF machines typically employ open slots. An experimental procedure was proposed, but not detailed, in which the rotor eddy-current losses are calculated via a power balance. Good correlation between the analytical and experimental results was observed.

In [9], Yamazaki et al. described their work involving the use of proprietary 3D FEA software to calculate rotor losses in both IPM and surface-mount permanent-magnet (SMPM) RF machines fitted with either NOW or conventional distributed windings. The FEA algorithm was verified experimentally by comparing torque and iron loss calculations (including both hysteresis and eddy-currents) to those obtained from measurements taken from an operating machine by a simple power balance. The primary results of the investigation are that the eddy current losses in a PM machine with NOW is much larger than that of an equivalent distributed winding machine and that the primary magnet eddy-current loss in an SMPM machine is a result of stator slot openings as opposed to stator current space harmonics.

3 Finite Element Analysis

Two-dimensional modeling for FEA is often preferred over its 3D counterpart during the design process of electric machines due to reduced complexity in the modeling and appreciably decreased computation time and resources. However, unlike the RF geometry, the AF machine is a naturally difficult geometry to model in two dimensions. Therefore, the purpose of this section is not only to detail any 2D and 3D FEA calculation results, but also to provide a description of the approach taken to modeling the AFPM machine in 2D. The software used for this analysis is Ansoft's Maxwell® where the transient solver is utilized in order to include the large-scale motion of the rotor passing over the stator slots. The results presented here have been computed for a 24-slot/20-pole single-sided AFPM with single-layer NOW (specific parameters match those of the machine on which experimental tests were performed, as given in Table 3).

3.1 2-D Modeling

The approach used to model the AFPM in two dimensions is to view the machine from the side (Fig. 1) and model it as a small portion of a radial-flux machine with a very large radius (on the order of 100 m). Depending on the slot-pole relationship of the machine, the model need only contain a fraction of the total machine (i.e. for the 24-slot/20-pole machine of considered here, the model contains 6 slots and 5 poles) where an appropriate symmetry multiplier in combination with master/slave boundary conditions are applied. The output parameters of the FEA (i.e. torques, etc.) can easily be converted from the large radial-flux machine reference frame to that of the smaller AFPM that is under consideration. It should be noted that this approach is necessary, as opposed to employing a model with strictly linear motion of the rotor, because the transient solver of the aforementioned software package is currently incapable of handling linear motion with master/slave boundaries.

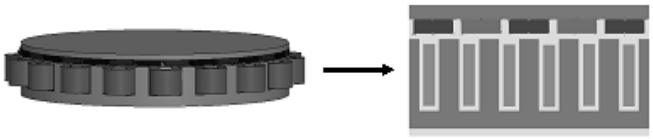

Fig. 1. Illustration of the 2D modeling of an AFPM machine.

In order to calculate the total eddy-current power loss in the rotor, the 2D FEA is run to determine the current density (J_z) in the magnets and rotor back-iron. The rotor power loss (P_r)

is then calculated as the integral over the material surface (*SA*) as shown in Eq. (1), where *h* is the model depth (z-direction), *m* is the symmetry multiplier (*m* = 4 for the 24-slot/20-pole machine), σ is the conductivity of the material.

$$P_r = hm \iint_{SA} \frac{|J_z|^2}{\sigma} dSA \qquad (1)$$

The analysis described was first conducted without a current input to the stator windings at various speeds in order to determine the rotor loss as a result of slotting alone. Then, the same procedure was performed for rotor speeds of 1000 and 2000 rpm with stator current set to provide selected values of output torque to be consistent with the experimental operating points as described in a subsequent section of this paper. The results of the 2D analysis are summarized in Table 1 and it is these estimations obtained via FEA that should be compared with experimental data.

Rotor Speed (rpm)	Output Torque (Nm)	Estimated Rotor Loss (W)
1000	0	1.8
1000	1.7	2.9
1000	2.7	4.4
2000	0	6.8
2000	1.7	10.1
2000	2.4	13.5
3000	0	14.8

Table 1. Rotor loss calculations resulting from 2D FEA.

3.2 3-D Modeling

Some comparison of the 2D FEA results with those of what is expected to be more accurate 3D results was deemed useful. However, due to the complexity and time consumption of running a transient simulation in 3D FEA, limited results will be presented here. Three full 3D simulations have been run to obtain values for $P_{r,slot}$ at speeds of 1000, 2000 and 3000 rpm. This was accomplished with a transient analysis in the aforementioned software employing large-scale rotor motion but null currents in the stator windings.

It has been the authors' experience that while macroscopic quantities (such as torques) will remain stable, more microscopic quantities (such as rotor loss) are quite sensitive to solver parameters such as mesh and time step sizes. In fact, quite erratic (and physically impossible) results have been found with meshing that is too coarse and inappropriate time stepping. The following rotor loss results have been obtained using the solver statistics detailed in Table 2 and though the symmetry rules used for the 2D FEA are equally applicable here, the simulations were performed using the entire machine model. Each simulation was carried out over a rotor rotation equal to one pole pitch and calculations were made at each of 100 time steps. The results of the 3D calculations for $P_{r,slot}$ are shown in Fig. 2 with average loss estimations of 1.3 W, 5.7 W and 8.3 W for rotor speeds of 1000, 2000 and 3000 rpm respectively.

Magnets	10000 tetrahedra
Rotor Back-iron	10000 tetrahedra
Stator Pole Faces	5000 triangles
Aspect Ratio	3
Nonlinear Residual Error	0.001

Table 2. Solver parameters used in the 3D FEA calculation of rotor losses.

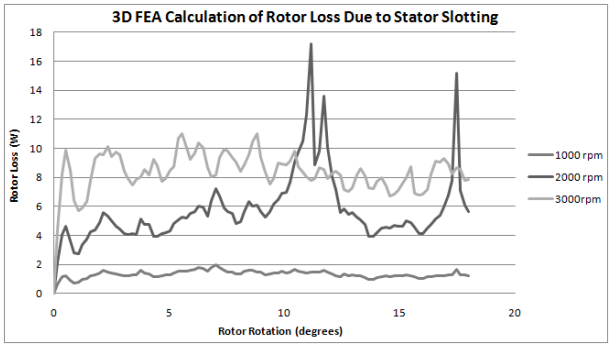

Fig. 2.3D FEA calculation of $P_{r,slot}$ for speeds of 1000, 2000 and 3000 rpm.

4 Experimental Measurement

The purpose of this section is to detail the experimental techniques used to isolate the rotor eddy-current loss. The methodology will be explained here, while the actual rotor loss determination (and comparisons with FEA calculations) will be addressed in the following section.

The test machine used for experimentation is a single-sided AFPM machine as pictured in Fig. 3 with parameters as described in Table 3. The problem of isolating the rotor losses is approached by running the test machine in generation mode via a drive motor coupled through an in-line torque transducer. Rotational speed measurement is made using a Hall-effect sensor and both voltage and current measurements are accessible for all three phase outputs of the generator. The power balance for this described arrangement is given by

$$P_m - P_e = P_{f+w} + P_{Cu} + P_{s,Fe} + P_{r,slot} + P_{r,NOW} \qquad (1)$$

where the, as yet undefined, power terms are:

P_m -- mechanical input power
P_e -- electrical output power
P_{f+w} -- friction and windage loss
P_{Cu} -- stator copper loss
$P_{s,FE}$ -- stator iron loss.

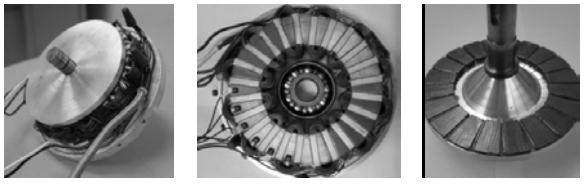

Fig. 3. Photographs of the single-sided AFPM used for experimentation.

Rated power	1 kW	*Slots*	24
Nominal speed	3000 rpm	*Poles*	20
Stator O.D.	110 mm	*Winding type*	NOW-single
Stator I.D.	66 mm	*Phase resistance*	1.3
Stator height	25 mm	*Phase inductance*	6 mH
Magnet type	NdFeB-N35	*Rotor thick.*	4 mm
Magnet thick.	4 mm	*Air-gap length*	1 mm

Table 3. Parameters of test machine used for experimental measurement of rotor losses.

4.1 No-Load Tests

The first no-load test that was run was to determine the spinning loss in the machine. This loss measurement encompasses P_{f+w}, $P_{s,Fe}$ and $P_{r,slot}$ and is accomplished through the setup described previously with the generator load disconnected. The measured spinning losses are shown in Fig. 4 for speeds ranging up to the rated speed of the machine. In order to obtain the best resolution possible at no-load, the torque transducer used in this setup is capable of measuring torques only up to 0.5 Nm.

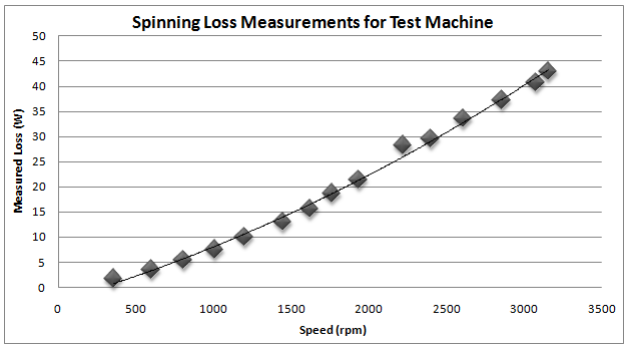

Fig. 4. Spinning loss measurements for test machine shown with a 2nd-order polynomial curve-fitting for the actual measured data points.

One concern that is often encountered when considering single-sided AF machines is the large axial load experienced by the bearing. Therefore, the second no-load test that was performed was to isolate the bearing friction loss, P_{f+w}, as a function of speed (note that the aerodynamic portion of this loss is ignored). In order to do so, the spinning loss measurement previously described was repeated using an uncut toroid as the stator piece (still fitted with a Hall-effect sensor for speed measurement). The airgap was increased such that the axial load on the bearing is equivalent to that of the actual machine, as computed in FEA. Fig. 5 shows the results of these measurements (that is, each point in the plot is an actual measured value). It can be argued that this measurement also contains a core loss component, however, as can be seen in Fig. 6, the increased airgap reduces the magnetic penetration depth into the core and the flux densities encountered are quite small; therefore, any core loss here is considered to be negligible.

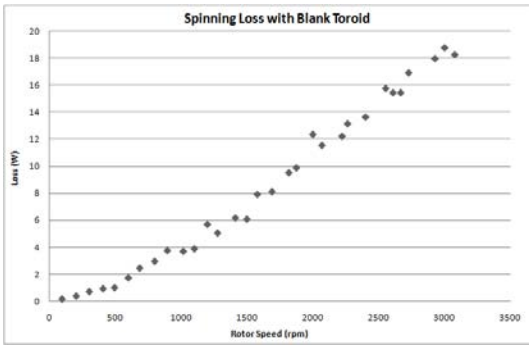

Fig. 5. Spinning loss measurements for test machine with uncut stator.

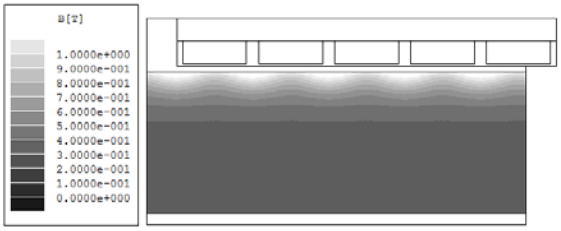

Fig. 6. 2D FEA representation of the stator flux densities present in the test machine with uncut stator.

4.2 Core Loss Measurements

Arguably the most challenging experimental measurement to isolate is the loss in the stator core. The stator of this particular test machine is constructed from a toroidal core consisting of tape wound 0.28 mm thick grade M4, grain-oriented silicon steel. In order to typify the behavior of the core loss under different operating conditions, the B-H curve of an uncut toroid was measured for a range of frequencies and magnetic induction levels.

The toroid was fitted with two sets of windings where the primary was connected to the output of an audio amplifier (driven with a sinusoidal signal generator) and the open-circuit voltage on the secondary circuit was directly measured and numerically integrated to obtain the flux density measurement. The specific core loss (W/kg) was then determined by numerical calculations on the B-H curve, scaled by the physical parameters of the toroid. This procedure was completed for frequencies ranging from 60 Hz to 500 Hz (corresponding to the fundamental frequency of the machine at rated speed) and induction levels from 0.6 T to 1.8 T. A sampling of the B-H curves is shown in Fig. 7 and the results of the loss calculations are given in Table 4.

The type of steel used in the stator of this machine is grain-oriented and the loss measurements described previously are made for flux in-line with the rolling direction of the steel. This is the true flux path in the stator back-iron of the machine; however, in the teeth, flux is pushed directly across the grain orientation and it is expected that the loss would increase in this case. According to [8] and [10], the specific loss is increased by a factor of approximately 2.8 when the flux path is 90^o from the rolling direction. It is this value that will be assumed when calculating the core loss, although a testing procedure is currently under way with the aim of

directly measuring this cross-grain loss. The ultimate goal of this core loss measurement procedure is to generate an input waveform for the amplifier to result in the exact temporal flux waveform (including harmonics) that truly exists in the back-iron and teeth of the machine. In this way, the core loss can be directly measured and calculations involving harmonic decomposition of the flux waveform are avoided.

2D FEA was used to identify that the magnetic induction levels present in the stator teeth and back-iron are 1.3 T and 0.8 T respectively. In terms of core size, the complete toroid has a mass of 1.15 kg where the total volumes of stator teeth and back-iron are 41% and 20% respectively, of the uncut toroid. Thus, for loss calculations, the back-iron mass is 0.23 kg and that of the teeth is 0.47 kg (total for all 24 teeth).

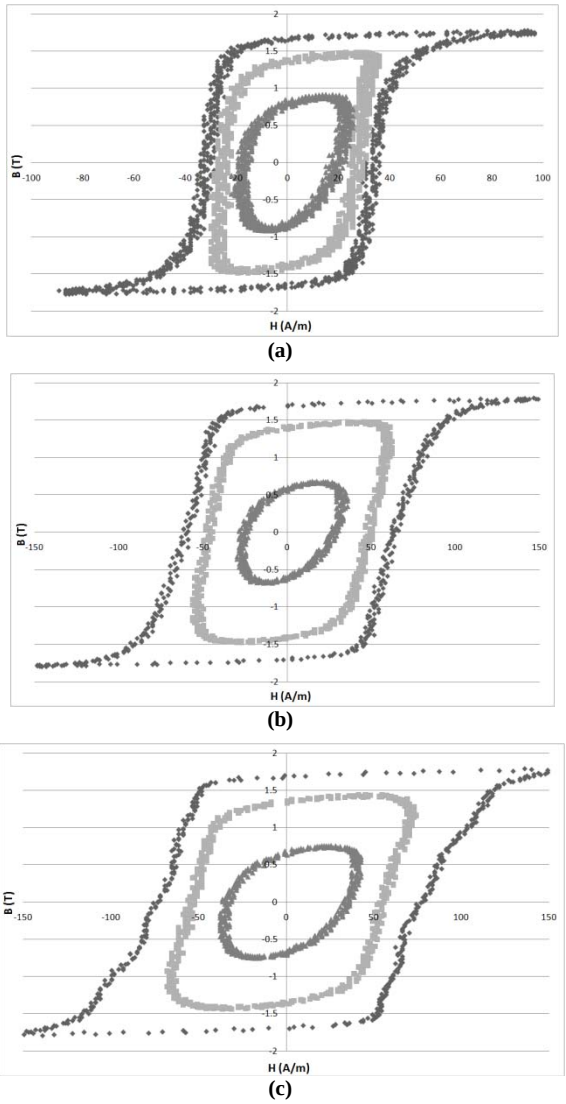

Fig. 7. B-H curves for the M-4 steel toroid used for the test machine stator construction at frequencies of (a) 100 Hz, (b) 300 Hz and (c) 400 Hz.

Using this physical data, the total core loss in the machine can be calculated as a function of fundamental frequency (or rotational speed). To this end, the data given in Table 4 along with 2nd-order polynomial curve fits for each frequency as a function of flux density was used to extrapolate values of specific loss at the induction levels of 1.3 T and 0.8 T. Thus, the core loss (W) as a function of machine speed is shown in Fig. 8.

Freq. (Hz)	Induction Level (T)	Specific Loss (W/kg)	Freq. (Hz)	Induction Level (T)	Specific Loss (W/kg)
60	1.8	***1.47***	300	1.8	***17.28***
60	1.5	***0.90***	300	1.5	***10.27***
60	0.8	***0.26***	300	0.7	***2.28***
100	1.8	***3.05***	400	1.8	***28.61***
100	1.5	***1.84***	400	1.4	***15.37***
100	0.9	***0.71***	400	0.8	***4.35***
200	1.8	***9.75***	500	1.5	***24.41***
200	1.6	***7.09***	500	1	***11.04***
200	1	***2.96***	500	0.6	***4.85***

Table 4. Experimental core loss data for the M-4 steel toroid that was used for the test machine stator construction for various frequencies and induction levels.

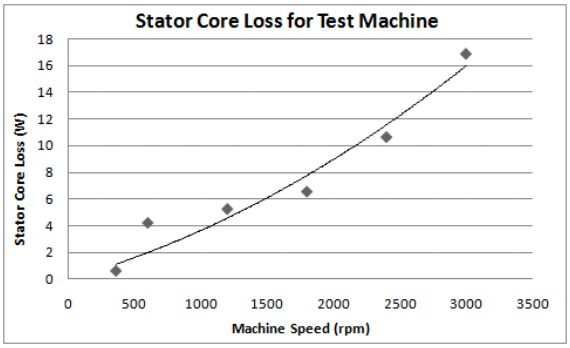

Fig. 8. Stator core loss for the test machine as a function of rotor speed. The points shown are extrapolated from actual measurement data using a 2nd-order polynomial curve fit.

4.3 Loaded Tests

The AFPM test machine was then run in generation mode, as previously described, with a variable resistive load connected. The loss measurements resulting from this test are shown in Table 5.

The total measured loss reported is the difference between P_{mech} and P_{elec} as in Eq.1. Simple i^2R calculations denote the conduction loss given in Table 5, where no discernible temperature rise was noticed in the stator windings.

Rotor Speed (rpm)	Output Torque (Nm)	Total Measured Loss (W)	Conduction Loss (W)
923	1.7	19.0	10.69
889	2.2	29.27	20.15
889	2.7	66.84	46.17
2000	1.7	46.92	10.86
2000	2.3	78.24	25.39
2000	2.5	93.22	31.63

Table 5. Sample results from experimental measurement of the test machine on-load.

5 Results and Conclusions

In this section, the experimental rotor eddy-current losses ($P_{r,slot}$ and $P_{r,NOW}$) are inferred from the previously described experimental measurements. Comparisons are also made with respect to the loss estimations obtained from FEA.

The rotor eddy-current loss that results from stator slotting alone ($P_{r,slot}$) can be isolated from the experimental measurements by subtracting the measured bearing loss and core loss (Fig. 9) from the spinning loss measurements given in Fig. 4. The equations found from curve-fitting are used to evaluate the spinning loss and core loss at rotor speeds exactly corresponding to the measured data points of the bearing loss to provide the plot of $P_{r,slot}$ as a function of rotor speed shown in Fig. 10. Also shown on the plot are the results obtained via FEA. It can be observed that the general shape of the 2D data points is systematic, but the values calculated for $P_{r,slot}$ are quite overestimated. For the 3D data, the calculated values are in better agreement with the experimental results, but the trend of the curve appears non-physical.

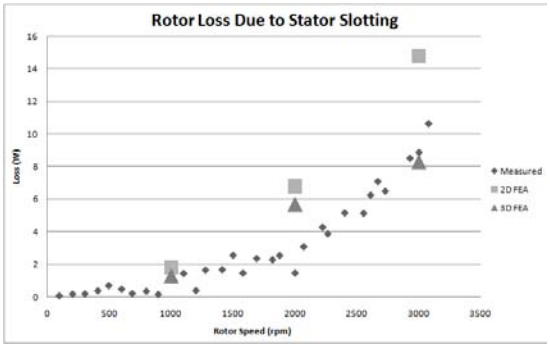

Fig. 10. Plot showing the relationship between $P_{r,slot}$ as inferred from experimental measurement and the estimated values obtained from 2D and 3D FEA.

Rotor Speed (rpm)	Output Torque (Nm)	$P_{r,NOW}$ Measured (W)	$P_{r,NOW}$ 2D FEA (W)
~1000	1.7	0.40	1.1
~1000	2.2	1.59	1.7
~1000	2.7	13.14	2.6
2000	1.7	12.46	3.3
2000	2.3	29.25	6.0
2000	2.5	37.99	6.7

Table 6. Comparison between $P_{r,NOW}$ as inferred from experimental measurement and the estimations obtained via 2D FEA.

The rotor eddy-current loss that exists as a consequence of the NOW scheme ($P_{r,NOW}$) is obtained from the experimental measurements of the machine on-load by subtracting the spinning loss (Fig. 4) and conduction loss from the total measured loss as given in Table 5. Note that the equation found from curve-fitting is used to evaluate the spinning loss at rotor speeds corresponding to the measured data points of the on-load testing. The results of this calculation are shown in Table 6 along with a reiteration of the 2D FEA estimations for comparison. 3D FEA calculations of $P_{r,NOW}$ are currently in progress, however no results have been obtained as of yet. The behavior of $P_{r,NOW}$, both as inferred from experimental measurements and estimated via 2D FEA, is as expected; however, there is a substantial discrepancy between the values obtained from the two methods.

6 References

[1] L. Alberti, E. Fornasiero, N. Bianchi, S. Bolognani, "Impact of Rotor Losses in a 12-Slot 10-Pole Axial Flux PM Machine", *IEEE Industry Applications Conference*, Oct. 2008.

[2] N. Bianchi, S. Bolognani, E. Fornasiero, "A General Approach to Determine the Rotor Losses in Three-Phase Fractional-Slot PM Machines", *IEEE International Conference on Electric Machines*, **Vol. 1**, May 2007, pp. 634-641.

[3] S. Han, T. Jahns, Z. Zhu, "Analysis of Rotor Core Eddy-Current osses in Interior Permanent Magnet Synchronous Machines", *IEEE Trans. on Industry Applications*, **Vol. 46**, Issue 1, Jan. 2010, pp. 196-205.

[4] A. Jassal, H. Polinder, G. Shrestha, C. Versteegh, "Investigation of Slot Pole Combinations and Winding Arrangements for Minimizing Eddy Current Losses in Solid Back-Iron of Rotor for Radial Flux Permanent Magnet Machines", *Proceedings of the International Conference on Electric Machines (ICEM)*, Sept. 2008, Paper ID 1292.

[5] R. Nuscheler, "Two-Dimensional Analytical Model for Eddy-Current Loss Calculation in the Magnets and Solid Rotor Yokes of Permanent Magnet Synchronous Machines", *Proceedings of the International Conference on Electric Machines (ICEM)*, Sept. 2008, Paper ID 1095.

[6] H. Polinder, M. Hoeijmakers, M. Scuotto, "Eddy-Current Losses in the Solid Back-Iron of PM Machines for Different Concentrated Fractional Pitch Windings", *IEEE International Conference on Electric Machines and Drives*, **Vol. 1**, May 2007, pp. 652-657.

[7] D. Saban, T. Lipo, "Hybrid Approach for Determining Eddy-Current Losses in High-Speed PM Rotors", *IEEE International Electric Machines and Drives Conference*, **Vol. 1**, May 2007, pp. 658-661.

[8] Soinski, M., "Application of the Anisometric Method for Determining Polar Curves of Induction, Apparent Core Loss and Core Loss in Cold-Rolled Electrical Sheets of Goss Texture", *IEEE Trans. on Magnetics*, **Vol. 20**, Issue 1, Jan. 1984, pp. 172-183.

[9] K. Yamazaki, Y. Fukushima, M. Sato, "Loss Analysis of Permanent-Magnet Motors with Concentrated Windings—Variation of Magnet Eddy-Current Loss Due to Stator and Rotor Shapes", *IEEE Trans. on Industry Applications*, **Vol. 45**, Issue 4, July 2009, pp. 1334-1342.

[10] http://www.kryfs.com/tech_articles.htm